IEEE Access
Multidisciplinary ⋮ Rapid Review ⋮ Open Access Journal

Received July 28, 2019, accepted September 17, 2019, date of publication September 30, 2019, date of current version October 11, 2019.

Digital Object Identifier 10.1109/ACCESS.2019.2944549

An EEMD-Based Electromagnetic Induction Method for Nondestructive Testing of Buried Metal Conductors

HENGLI SONG[1,2,3], HAOBIN DONG[1,2,3], ZHIWEN YUAN[3], JUN ZHU[3], HAIYANG ZHANG[3], AND YUJIN HUANG[1,2]

[1]School of Automation, China University of Geosciences, Wuhan 430074, China
[2]Hubei Key Laboratory of Advanced Control and Intelligent Automation for Complex Systems, Wuhan 430074, China
[3]Science and Technology on Near Surface Detection Laboratory, Wuxi 214035, China

Corresponding author: Zhiwen Yuan (zhiwen_yuan@163.com)

This work was supported in part by the Foundation of Wuhan Science and Technology Bureau under Grant 2017010201010142, and in part by the Foundation of Science and Technology on Near-Surface Detection Laboratory under Grant TCGZ2017A001.

ABSTRACT Nondestructive testing of substation grounding grids is an issue that has increasing importance. The traditional EMI method transforms the condition of the undergrounding conductors to the surficial induced electric signal in the sensing coil. However, The EMI signals excited by multiple coexisted faults combining with other unknown noises surrounding the substation often cause the failure of detection. Therefore, the observed EMI signals rather complex and cannot be used directly. To address this problem, the separation of individual signatures from the mixture is posed as an SCBSS problem. To extract the induced signal, an EEMD-based EMI method is proposed. The desired signal is then reconstructed to visualize the structure of the grounding grids by a virtual instrument that consists of DAQ and digital signal processing modules. The numerical simulation and practical experiments are employed. The results show the proposed method can be used to effectively detect the topological structure of grounding grid in real substations' electromagnetic environment.

INDEX TERMS Grounding grid, electromagnetic induction (EMI), ensemble empirical mode decomposition (EEMD), single channel blind source separation (SCBSS), nondestructive testing (NDT).

I. INTRODUCTION

The grounding system is a critical factor to an electrical substation. It ensures operational performance of the equipment and safety of personnel on site. The main element of a grounding system is a mesh of interconnected metal conductors which provides a low resistive path for the surge currents to flow into the earth. In general, the grounding grid is made of metal or metal alloys such as steel, galvanized steel and copper being horizontally buried about 0.3-2m deep under the soil [1]. The buried mesh of bare metal conductors spread over the whole area of the substation. Vertical ground rods are connected to the grid at various positions of the substation such as lightning arresters and power transformers. These vertical conductors are the only access points to the buried horizontal conductors.

The buried metal conductors are subjected to corrosion which is a common natural phenomenon. Due to long-term soil corrosion, some metal branches may even become broken [2]. Corrosion is the most dangerous factor that severely threatens the reliability and integrity of the grounding grids. Therefore, there is an urgent need to conduct an efficient diagnosis method to evaluate the status of the grounding grids. However, in an operating substation, the topological structure of the grounding grid is often unknown and uncertain due to human error. Therefore, detecting the topology of the grounding grid is a prerequisite for detecting corrosion and breakpoints.

In recent years, an increasing number of scholars proposed nondestructive testing (NDT) methods to the corrosion and breakpoint diagnosis of grounding grids [3]. At present, these NDT methods can be classified into three main categories. They are the equivalent circuit network method [4], [5], the electrochemical method [6] and the electromagnetic induction (EMI) method [7]–[9].

The associate editor coordinating the review of this manuscript and approving it for publication was Zhengqing Yun.

The equivalent circuit network method regards the grounding grids as a pure resistance network and establishes the diagnosis equation that describes the nonlinear relationship among branch resistances and node voltages. However, the variations of the grounding resistance and the surface potential are quite small and undetectable in the early stage of corrosion of conductors. The electrochemical method often fails due to the low signal to noise ratio (SNR). Moreover, this method is invalid for conductor breaks detection.

As one of the geophysical methods, the EMI method is most widely used to measure the topological structure and the break position of the grounding grids [10]–[12]. In theory, the EMI method can detect the degree of corrosion in the case where the grounding network topology is unknown. This method injects current into two down-lead wires of the grounding grid and measures the surface magnetic flux density induced by the metal conductors. The distribution of the electromagnetic reveals the topological structure and broken points of grounding grids.

Reference [13] measured the topological structure of the grounding grid by injecting a DC current into two conductors of the mesh. The derivative of surface flux density in a systematic order was used to find the position of the grid. Further works in [14] applied the derivative method to diagnose breaks in grounding grids without excavation. More simulations and lab experiments were carried out in [15]. The results showed the feasibility of the EMI and the derivative method.

The fundamental problem in the EMI method is to accurately extract the small induced signal from the sensing coil. However, the sampled signal is usually a mixture of several signals due to the noisy electromagnetic interference surrounding the substation [16]. This often causes the failure of detection. Moreover, typical filters are noneffective because the amplitude of the strong interference is usually tens of times of the wanted signal.

Since the sampled signal of EMI is an unknown mixture of multisource, it is necessary to separate the induced signal from other signals. This problem can be posed as a blind source separation (BSS). BSS separates the mixed signals without knowing the prior knowledge of the number of source signals and the mixed path [17].

Independent component analysis (ICA) is the most used algorithms to realize BSS [18]. More improved ICA algorithms, such as FastICA and ASS-GAICA [19], have been proposed by researchers to enhance the applicability of the ICA in various fields.

Especially, single channel blind source separation (SCBSS) can separate the source signal with only one observed signal [20]. Among SCBSS methods, empirical mode decomposition (EMD) has a highly adaptive nature in extracting features [21]. EMD is nonparametric in decomposing empirically sensing signal into a series of intrinsic mode functions (IMFs) [22]–[24]. The advantage of the EMD allows the nonstationary and nonlinearity information of the signal to be revealed for accurate characterization of signals [25], [26].

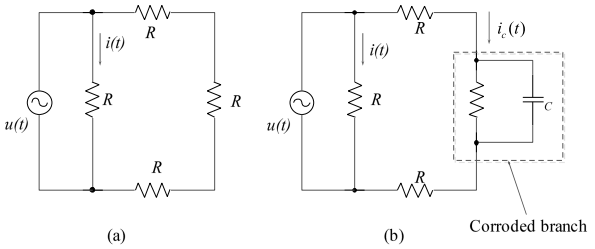

FIGURE 1. Equivalent circuits of normal and corroded mash.

However, EMD often fails to extract features accurately because of mode aliasing [27].

To alleviate mode mixing and aliasing, the ensemble empirical mode decomposition (EEMD) was developed to improve EMD [28]. EEMD can decompose a complicated signal into a series of IMFs according to the signal local characteristics. By adding noise to the original signal and calculating the means of IMFs repeatedly, the EEMD method can avoid the mode mixing problem in all cases.

In order to obtain accurately the surface distributions of the magnetic field in the intense electromagnetic environment of substations, an EEMD-EMI method is proposed to improve the anti-noise ability of the traditional EMI method. the EEMD decomposes adaptively the EMI sequences adapted from the time-frequency domain analysis method. The proposed method is applied to detect the topological structure of the grounding grids in a real substation. And the positions of buried metal conductors of the grids are successfully detected with it.

This paper is organized as follows. The measuring principle of traditional EMI and the frame diagram of the NDT system are presented in Section 2. The EEMD algorithm is briefly described in Section 3 following by the proposing of the EEMD-EMI method. Section 4 and Section 5 describe the numerical simulation and the practical experiments respectively. Finally, conclusions are given in Section 6.

II. TRADITIONAL EMI METHOD TO NDT OF GROUNDING GRIDS

A. PRINCIPLE OF THE TRADITIONAL EMI METHOD

The EMI method is to detect the grounding grids by measuring the spatial distribution of the magnetic field induced by grounding conductors which are excited by an alternating current. The magnetic distribution can provide useful information for the topology and position of conductors.

When rust does not occur in any branches of a grounding grid, the topological structure of the grounding grid remains unchanged. The equivalent circuit of a mesh of the grounding grid is shown in Fig. 1.

The output function of the excitation source is denoted as

$$u(t) = U \cos \omega t \tag{1}$$

where U is the magnitude, ω is the angular frequency.

We suppose the resistances of each branches are all R.The current flowing in one of the conductor branches can be

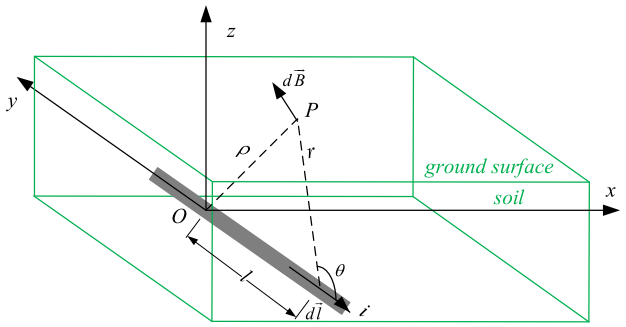

FIGURE 2. Differential magnetic field of a current-carrying conductor.

written as

$$i(t) = \frac{U\cos\omega t}{R} \tag{2}$$

According to electromagnetic induction theory, when a current in sine wave flows along the metal conductors of grounding grids, an AC magnetic field is created in the same frequency. The magnitude of the magnetic field is the function of the carrying current intensity.

To simplify the problem, consider a single current-carrying conductor buried in the soil and on the y-axis as shown in Fig. 2. The current I flows through the conductor and the point P is on the ground.

The differential magnetic field in an arbitrary point on the surface ground of the conductor branch can be written as

$$d\vec{B} = \frac{\mu_0}{4\pi}\frac{i(t)d\vec{l}\times\hat{r}}{r^3} = \frac{\mu_0}{4\pi}\frac{i(t)dl\sin\theta}{r^2} \tag{3}$$

where μ_0 is the magnetic conductivity. $d\vec{l}$ is the differential element of the conductor. r is the distance from P to the $d\vec{l}$. $\hat{r}$ is the direction vector of the r. θ is the angle between $d\vec{l}$ and $\hat{r}$.

Therefore, the magnetic flux density of a current-carrying straight conductor is

$$\vec{B}(t) = 2\int_0^\infty d\vec{B} = \frac{\mu_0 i(t)}{2\pi}\int_0^\infty \frac{\sin\theta dl}{l^2+\rho^2} \tag{4}$$

where ρ is the vertical distance from P to the conductor. l is the distance between O and $d\vec{l}$. Other notations are shown in Fig. 2.

Knowing that $\sin\theta = \sin(\pi-\theta) = \frac{\rho}{\sqrt{l^2+\rho^2}}$, we have

$$\vec{B}(t) = \frac{\mu_0 i(t)}{2\pi\rho}\left[\frac{l}{(l^2+\rho^2)^{1/2}}\right]_0^\infty = \frac{\mu_0}{2\pi\rho}\cdot\frac{U\cos\omega t}{R} \tag{5}$$

If the metal conductors either completely or partly become oxides, meaning a fault of the grounding grid, the AC impedance of the corroded segment deviates from the original value. The equivalent circuit of a corroded conductor is modeled as the parallel circuit of a resistance and a capacitance, shown as Fig. 1(b). Let λ be the cross-sectional area proportion of the corroded conductor. The impedance of the corroded conductor turns to be

$$Z_c = \left(\frac{(1-\lambda)}{R} + j\omega C\right)^{-1} = \frac{R}{1-\lambda+j\omega RC} \tag{6}$$

The variation of the impedance leads to the variation of the current in the corroded conductor which can be written as

$$i_c(t) = \frac{U\cos\omega t}{Z_c} = \frac{(1-\lambda+j\omega RC)U\cos\omega t}{R} \tag{7}$$

Consequently, the surficial magnetic flux density above the corroded branch of the conductor becomes

$$\vec{B}_c(t) = \frac{\mu_0}{2\pi\rho}\cdot\frac{(1-\lambda+j\omega RC)U\cos\omega t}{R} \tag{8}$$

Comparing (5) with (8), we can see that the variation of the impedance reforms the distribution of the magnetic field on the ground surface above the corroded segment. Therefore, by establishing the relation between the surficial magnetic flux density and the fault, the corroded points of the grounding grid can be diagnosed and located through the electromagnetic method.

In this work, the induced electromagnetic field is measured by the designed receiver which includes a sensing coil of wire. The coil is set above the ground surface of the grid.

The surficial magnetic flux density $\vec{B}$ by arbitrary current-carrying conductor can be decomposed into the horizontal component B_H and vertical component B_V which are respectively written as follows.

$$|B_H| = \left|\vec{B}\right|\cos\delta \tag{9}$$

$$|B_V| = \left|\vec{B}\right|\sin\delta \tag{10}$$

where δ is the angle between the magnetic line of force and the horizontal direction. When the axial direction of the coil is set to be horizontal, the coil is inducted by the horizontal component of the surficial magnetic flux. According to Faraday's law of induction, the induced AC voltage ε in the sensing coil generated by the time-varying surficial magnetic field is as follows.

On normal branches

$$\varepsilon = \frac{\mu_0 NS}{2\pi\rho}\cdot\frac{U\omega\sin\omega t\cos\delta}{R} \tag{11}$$

On corroded branches

$$\varepsilon_c = \frac{\mu_0 NS}{2\pi\rho}\cdot\frac{(1-\lambda+j\omega RC)U\omega\sin\omega t\cos\delta}{R} \tag{12}$$

where N is the number of windings in the coil. S is the cross-sectional area of the coil.

Equation (11) illustrates that the EMI method can be used to detect the position of each conductor in the underground, thereby further obtaining the topological structure of the grounding grid. Equation (12) provides the theoretical basis for detecting the breakpoints and corrosion degree of the grounding grid.

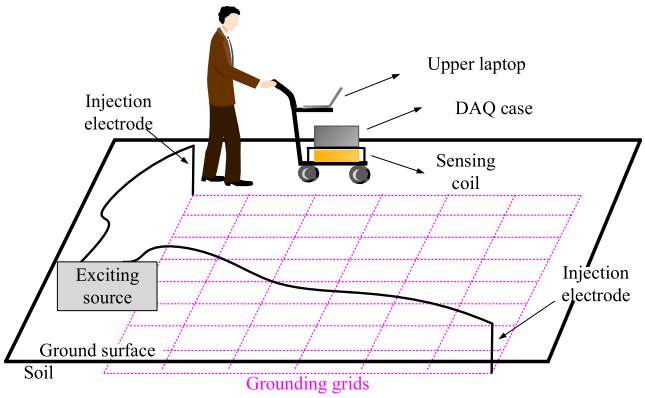

FIGURE 3. Frame diagram of the NDT system.

The EMI response measured from the sensing coil is a complex-valued quantity. Its real part is termed the ''in-phase'' (IP) component while the imaginary part is termed the ''quadrature'' (Q) component. The in-phase and quadrature components at each frequency of interest are obtained by convolving the received time-series with a sine time-series (for in-phase) and a cosine time series (for quadrature) at each frequency of interest.

B. FRAME DIAGRAM OF THE NDT SYSTEM

The frame diagram in Fig. 3 outlines the proposed strategy intended for nondestructive testing of buried metal grids. A transmitter-receiver pair composes the NDT system. The diagnosis procedure is as follows. The transmitter firstly provides an excitation current directly into grounding grids through two injection electrodes of the grounding grids. Then the receiver measures the surficial magnetic induction density developed by current-carrying conductors. Consequently, the corrosion conditions or breakpoints of the mesh conductors are confirmed by analyzing the distribution characteristics.

The surficial induced magnetic field measurement is performed for the detection of the grounding grids. The transmitter supplies the exciting current at a well-designed and settled frequency. The sine wave current energizes the grounding grid continuously and creates the magnetic field on the surface ground. In order to measure the magnetic field, a sensing coil is arranged on the surface of the ground in fixed height. The direction of the coil's axis is set horizontally. The induced AC voltage in the coil is measured by the receiver which involves sensing coil, analog conditioning circuit, and the PC-based virtual instruments.

In our previous work [29], the EMI-based NDT equipment operated well and obtained satisfactory results on a small physical model of metal grids in our laboratory. The position and the topological structure can be detected accurately. However, the traditional EMI method was unsuccessful in practical application in real substations because of the strong interference and harsh electromagnetic environment around the detecting area.

The strong interference around the substation is mainly generated by multisources such as main power transformers, high-speed on-off controllers, high voltage reactors, switches, current-carrying cables, and busbars. The frequency components of the interference are various and stochastic.

According to our field measurement, the induced voltage in the sensor generated by the interference signals is up to more than a dozen volts while the amplitude of the wanted signal is hundreds of mV. The amplitude of the interference is nearly one hundred times the amplitude of the wanted signal. The NDT equipment is in a ''harsh'' electromagnetic environment.

The traditional anti-noise means, such as analog and digital filter, power frequency notch filter and adaptive filter, were attempted in our previous work. The result was still unsatisfying.

To solve the problem, the convenience of EEMD on de-noising is combined with the EMI to the EEMD-EMI method. In the following section, the principle of the EEMD is described and the EEMD-EMI method is proposed.

III. THE PROPOSED EEMD-EMI METHOD

A. BRIEF DESCRIPTION OF EEMD

The noise could be induced by local intermittent instabilities or irresolvable subgrid phenomena, or generated by some concurrent processes in the environment in which the investigations are conducted. The observed signal is a mixture of true signal and noise from unknowing sources in the practical application of detection of grounding grids, i.e.,

$$x(t) = AS(t) + N(t) \tag{13}$$

where $x(t)$ denotes the observed signal. A is the mixing matrix. $S(t)$ and $N(t)$ represent multiple source signals and noise signals respectively.

EMD, as a statistical signal processing, is a very useful tool for signal detection. As mentioned before, EMD's most significant drawback is mode mixing which implies false components in IMFs. In practical applications, the collected EMI signal contains a certain amount of random noise or gaps. In this condition, the decomposition is usually unstable and does not satisfy the physical uniqueness. To overcome the shortcoming of EMD, EEMD utilizes the EMD's scale separation ability and statistical features to segment the signal by a noise assisted analysis method, whereby EMD is applied to every member of the ensemble:

$$s_m(t)\Big|_{m=1}^{M} = x(t) + w_m(t)\Big|_{m=1}^{M} \tag{14}$$

where $w_m(t)\big|_{m=1}^{M}$ are independent realizations of white noise.

With the help of EMD, the contaminated signal $s_m(t)\big|_{m=1}^{M}$ can be decomposed into a series of IMFs as

$$\widehat{x}(t) = \sum_{n=1}^{N} c_n(t) + r(t) \tag{15}$$

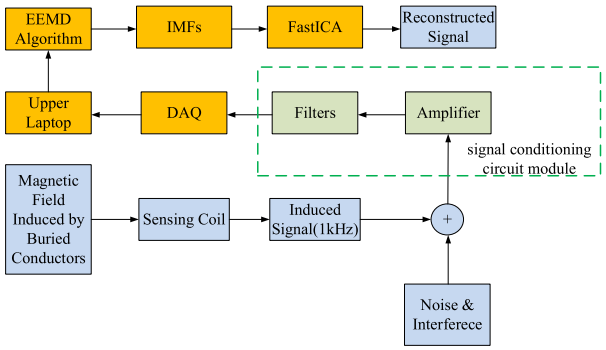

FIGURE 4. Block diagram of the EEMD-EMI method.

where $c_n(t)$ is an IMF, n represents the sequence of each IMF. N is the number of IMFs. $r(t)$ is the residue of data $x(t)$, after n number of IMFs are extracted.

After iteration, the final IMFs are

$$c_n(t) = \frac{1}{M}\sum_{m=1}^{M} c_{n,m}(t) \tag{16}$$

Thus the noisy sampled signal is split into a sum of modes for further processing.

B. EEMD-BASED EMI METHOD

The receiver of the NDT system has only one sensing coil, therefore the induced signal is sampled by a single-channel data acquisition. As one of SCBSS method, EEMD has been widely used in processing dynamic data and has made great achievements. We adopt EEMD on EMI data to effectively reduce the influence of interference and outliers to obtain stable performance. The improved EMI method basing on EEMD is shown in Fig. 4.

The EMI signals thus acquired by the receiver were amplified using a differential amplifier, and filtered with an analog band-pass filter respectively. In the next step, the amplified signals were sampled at a rate of 100kHz and digitized with a DAQ device which samples a time series of the induced voltage in the coil. The sampling rate is 100 times the frequency of the original signal. The true signal $\varepsilon(t)$ is relatively weak and buried in harsh EME of substations. The EEMD algorithm is implemented in the upper laptop to extract the weak induced signal in coil from the harsh electromagnetic environment. Upon being supplied with the single-channel EMI signal in the sensing coil, the EEMD decomposes the input into IMFs, which in turn are separated. The amplitude of the magnetic field is calculated from the reconstructed voltage signal.

The signal processing procedure is as follows, shown in Fig. 5.

1) Sample a time series of the induced voltage in the coil. The sampling rate is 100 times the frequency of the original signal. The true signal $\varepsilon(t)$ is relatively weak and buried in harsh EME of substations. The original sampled signal can

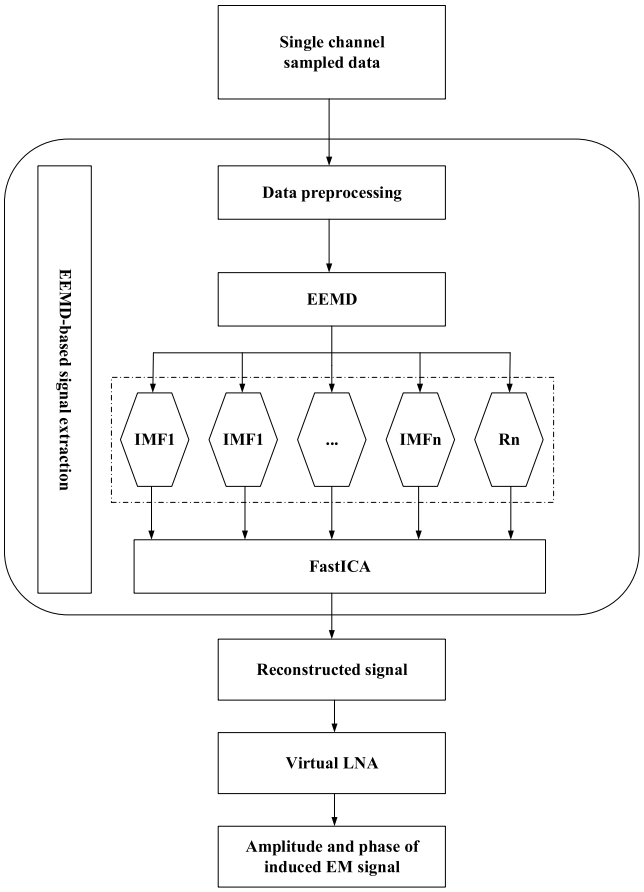

FIGURE 5. EEMD-based EMI signal extraction process.

be described as

$$\delta_0(t) = \varepsilon(t) + N_p(t) \tag{17}$$

where $N_p(t)$ is a serial of unknown sources and noises.

2) Add a serial of white noises to the original sampled data. Denote the serial of white noises as $\{n_1(t), n_2(t), \ldots n_m(t)\}$, then the sampled signal turns to

$$\begin{cases} \delta_1(t) = \delta_0(t) + n_1(t) \\ \delta_2(t) = \delta_0(t) + n_2(t) \\ \ldots \\ \delta_m(t) = \delta_0(t) + n_m(t) \end{cases} \tag{18}$$

3) Implement EMD on each $\delta_i(t)\,|i = 1, 2, , \ldots, m$. The detail process is as follows.

(a) Extract the local maxima and minima of $\delta_i(t)$. Interpolate the local maxima and the minima cubic spline lines to form upper and lower envelops of $\delta_i(t)$, denoted as $\gamma_{up}(t)$ and $\gamma_{low}(t)$ respectively.

b) Calculate the mean of the upper and lower envelops as

$$m_{i,1}(t) = \frac{\gamma_{up}(t) + \gamma_{low}(t)}{2} \tag{19}$$

(c) Obtain a new series by

$$h_{i,1}(t) = \delta_i(t) - m_{i,1}(t) \tag{20}$$

If $h_{i,1}(t)$ is an IMF, Let $h_{i,1}(t)$ be the first IMF of $\delta_i(t)$. Otherwise go to next step.

(d) See $h_{i,1}(t)$ as original signal, repeat (a)∼(c).

$$h_{i,2}(t) = h_{i,1}(t) - m_{i,1}(t) \tag{21}$$

Repeat k times to obtain

$$h_{i,k}(t) = h_{i,k-1}(t) - m_{i,k-1}(t) \tag{22}$$

(e) Denote $c_{i,1}(t) = h_{1,k}(t)$, $c_{i,1}(t)$ is the first IMF of $\delta_i(x)$

Repeat (a) ∼ (e) to obtain all the $c_{i,j}(t)\,|i = 1, 2, \ldots, m; j = 1, 2, \ldots, n$.

Define

$$r_i(t) = \delta_i(t) - c_{i,n}(t) \tag{23}$$

is the residue of the signal.

Thus the sampled signal can be written as

$$\delta_i(t) = \sum_{j=1}^{n} c_{i,j}(t) + r_i(t) \tag{24}$$

4) Implement EMD to all the $\delta_i(t)$. Obtain m IMFs and m residues, written as

$$C = \begin{bmatrix} c_{1,1} & c_{1,2} & \ldots & c_{1n} \\ c_{2,1} & c_{2,2} & \ldots & c_{2,n} \\ \ldots & \ldots & \ldots & \ldots \\ c_{m,1} & c_{m,2} & \ldots & c_{m,n} \end{bmatrix}, res = \begin{bmatrix} r_1 \\ r_2 \\ \ldots \\ r_m \end{bmatrix} \tag{25}$$

5) Calculate the mean of C and res, written as

$$\begin{cases} C_1 = \dfrac{1}{m}\displaystyle\sum_{i=1}^{m} c_{i,1} \\ C_2 = \dfrac{1}{m}\displaystyle\sum_{i=1}^{m} c_{i,2}, RES = \dfrac{1}{m}\displaystyle\sum_{i=1}^{m} r_i \\ \ldots \\ C_n = \dfrac{1}{m}\displaystyle\sum_{i=1}^{m} c_{i,n} \end{cases} \tag{26}$$

The original signal can be written as

$$\widehat{\delta_0}(t) = \sum_{i=1}^{n} C_i + RES \tag{27}$$

6) After EEMD is performed and a set of averaged IMFs is derived, FastICA is applied to the whole set of IMFs. The ICs are extracted as well as the mixing and separation matrices, A and W. After selecting the ICs of interest, the signal is reconstructed first by multiplying it by the mixing matrix to derive a new IMF set, in which only the IC of interest is present. Summing over the newly derived IMF set the appearance of the desired source in the original signal is obtained.

7) The result of step 6) is used to calculate the amplitude and phase of the induced signal by a virtual LNA in the upper notebook. The position and the corroded point of the buried conductor can be determined according to the distribution of the amplitude and phase of the induced electromagnetic field.

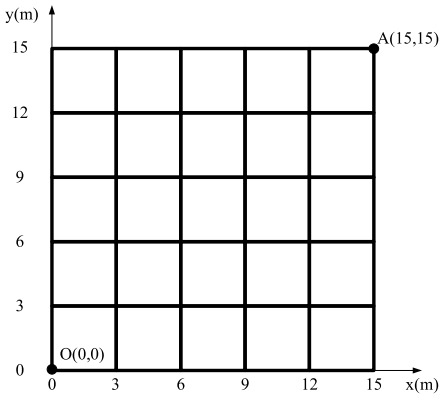

FIGURE 6. Simulation model of grounding grid in regular shape.

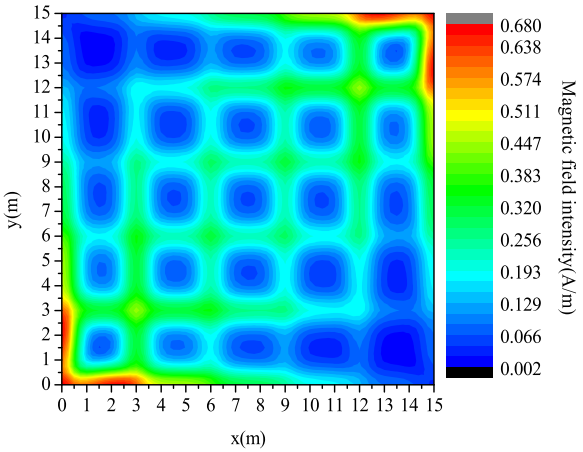

FIGURE 7. Surface magnetic field intensity distribution of regular grid.

IV. NUMERICAL SIMULATION

A. SIMULATION OF THE EMI METHOD

The simulations of the EMI method are performed in CDEGS software. The numerical model considered for simulation analysis is made up of steel with buried depth of 0.8m. All conductors are 5mm in diameter. In order to verify the correctness of the EMI method, two grounding grid models with different shapes and sizes are established.

The first model is a regular mesh with dimensions equal to 15m × 15m as shown in Fig. 6.

The physical model has 5 × 5 square-shaped grids, each of them is in size of 3m ×3m. An AC sinusoidal excitation current of 1kHz, 10A is injected into the points O (0,0) and A (15, 15).

The induced magnetic field intensity of the grounding grid is calculated by the module in CDEGS. The surface magnetic field intensity distribution color map is shown in Fig. 7.

It can be seen from the figure that the distribution of the ground magnetic field is completely consistent with the position and the topological structure of the grid.

To verify the feasibility of the EMI method on an irregular grid, we built another simulation model as shown in Fig.8. The model is a complicated mesh with dimensions equal to 20m × 20m.

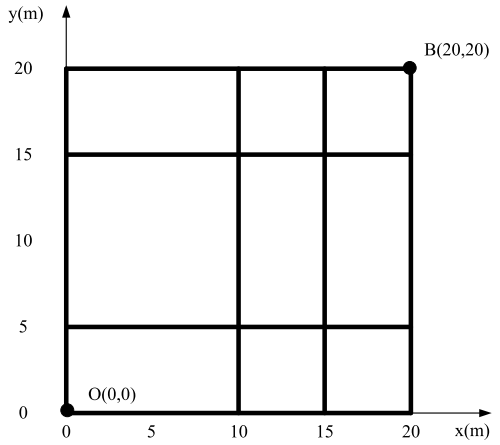

FIGURE 8. Simulation model of grounding grid in irregular shape.

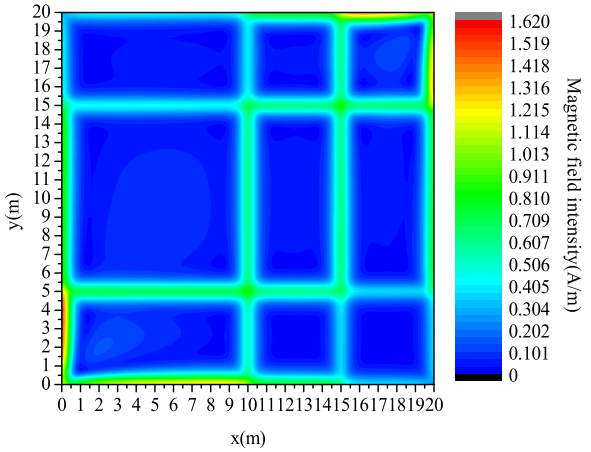

FIGURE 9. Surface magnetic field intensity distribution of irregular grid.

An AC sinusoidal excitation current of 1kHz, 10A is injected into the points O (0,0) and B (20, 20). The other simulation conditions and parameters are similar to the previous model. The topological structure of the grounding grid is revealed clearly by the magnetic field distribution, shown in Fig.9.

The above results of simulations verify the correctness of the EMI method even the topological structure of the grounding grid is irregular mesh. In practical application, the magnetic field intensity needs to be measured accurately to obtain a clear topological structure. Therefore, the sinusoidal EMI signal in the sensing coil must be extracted from the complex electromagnetic interference.

B. SIMULATION OF THE EEMD-EMI METHOD

The purpose of this subsection is to verify the proposed method can effectively separate the multisource mixed EMI signal. The simulation signals consist of four sources: the wanted signal $a(t)$, the unwanted signals ($b(t)$ and $c(t)$) which are in lower frequencies representing electromagnetic interference in the measuring environment. The other simulated signal $n(t)$ is the Gaussian noise,

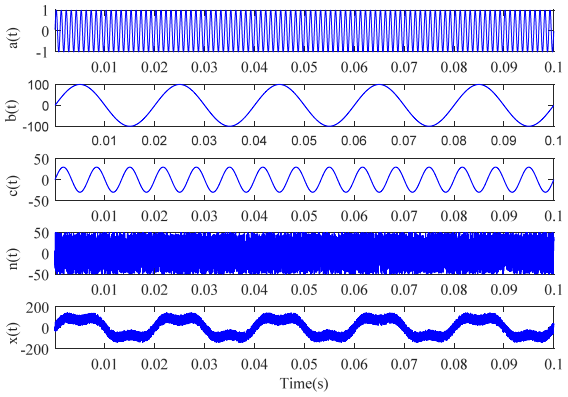

FIGURE 10. Simulated sources and mixed signal.

i.e. $S(t) = [a(t), b(t), c(t), n(t)]^T$, and more specifically:

$$\begin{cases} a(t) = \sin(2\pi f_1 t) \\ b(t) = 100\sin(2\pi f_2 t) \\ c(t) = 30\sin(2\pi f_3 t) \\ n(t) \sim 100N(0, \sigma^2) \end{cases} \tag{28}$$

where $f_1 = 1000$Hz which equals the frequency of the driving AC current in the buried conduction, $f_2 = 50$Hz which is the frequency of the power line interference, $f_3 = 150$Hz which is the frequency of the third harmonic of power line, and the Gauss noise intensity can be determined by controlling the standard deviation. The sources and the mixed signal are shown in Fig. 10.

Suppose the signal sampling frequency of a single sensor is 100k Hz, and the signal length is 10000 sampling points. The noise parameter σ is 0.1.

In order to simulate the collected signal with strong noise, the amplitudes of $b(t)$, c(t) and $n(t)$ are much larger than $a(t)$, respectively are 100, 30 and 100 times of $a(t)$. As the plot of the mixed signal $x(t)$ which is a single-channel observed signal, the desired signal is buried in the other ones.

The EEMD algorithm is used to decompose the mixed signal. The result of the decomposition is shown in Fig. 11.

Then combining the obtained IMFs into a multidimensional observation signal. Use FastICA to reconstruct the original signal, as shown in the first independent component (IC1) of Fig. 12.

Comparing $a(t)$ of Fig. 10 with IC1 of Fig. 12 the time domain oscillogram of the estimated signals and the source signals are basically similar. This indicates the source signals are nicely captured.

V. PRACTICAL EXPERIMENTS

A. DEVELOPMENT OF THE NDT EQUIPMENT

The EMI signal is achieved from our self-made NDT equipment as shown in Fig. 13.

The equipment, settled in a customized trolley, consists of three main part: the sensing coil, the mainframe case which includes a signal conditioning circuit module and a

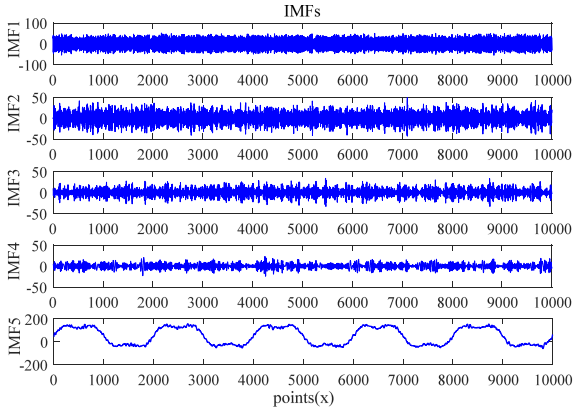

FIGURE 11. Decomposition results of mixed signal by EEMD.

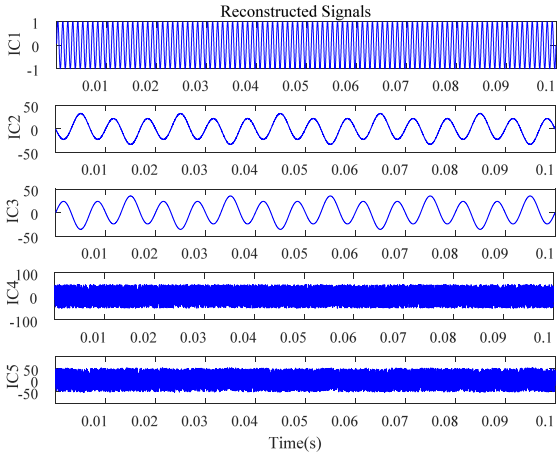

FIGURE 12. Reconstructed signals.

DAQ module, and the upper laptop. There is a photoelectric rotary encoder on the axis of the left rear wheel of the trolley. The whole trolley can be pushed easily on the surface of the substation's area to inspect the EMI signal of the undergrounded conductors. The photoelectric rotary encoder records the moving distance of the trolley and triggers the sampling of the DAQ per 50cm.

One sensing coil is used to acquire the EMI signal. The EMI signal is transformed into an AC voltage signal which is processed by an analog conditioning circuit. The signal conditioning circuit includes a differential preamplifier, a programmable band-pass filter and the main amplifier. The center frequency of the filter is digitally set to be 1kHz which is similar to the frequency of the AC excitation current.

After regulated the original signal is sampled by a well-designed DAQ module which is connected to the upper laptop. The DAQ is developed on DAQmx data acquisition software. The panel of the equipment is based on LabVIEW running on the laptop. The DAQ performs anti-aliasing filtering, A/D conversion, etc. on the sampling signal and finally converts the analog voltage signal into digital data. The sampling frequency is programmed to be 100kHz which is 100 times of the wanted signal. The number of sampling

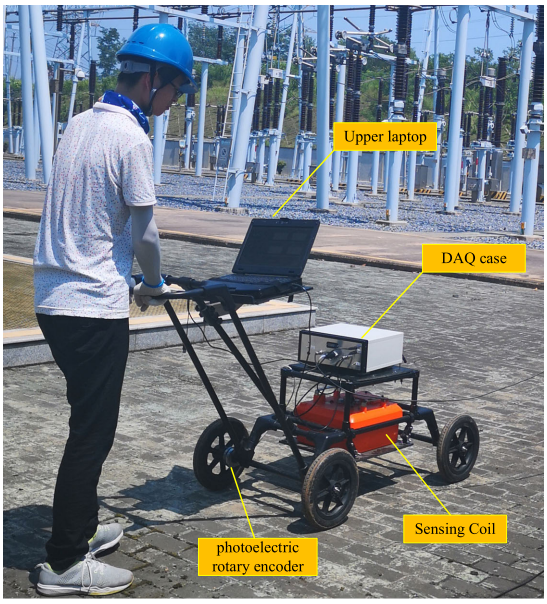

FIGURE 13. A demonstration of NDT equipment for grounding grids.

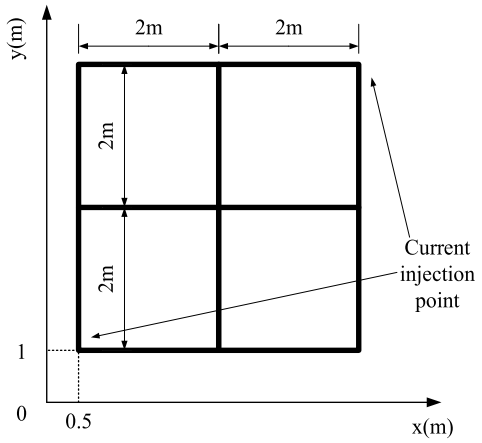

FIGURE 14. Small physical model of grounding grid.

points is 1000. The original sampled time domain data is then transmitted to the computer for storage and further process.

The sampled data is consequently proposed by the proposed EEMD algorithm. According to the reconstructed data, the topological structure and the position of the corroded points are calculated and displayed in a 3D view.

B. EXPERIMENTS ON A SMALL MODEL OF GROUDING GRID

A scale-down grid model made of galvanized flat steel was built to implement the experiment. As shown in Fig. 14, the metal grid features a 4m×4m rectangle with 4 meshes. The buried depth of the grounding grid is near the surface. In order to imitate the actual burying depth, the operation height of the coil to the surface is 0.3m.

The sinusoidal current (2A, 1kHz) is injected from node A and flows out from node B. Since the network structure

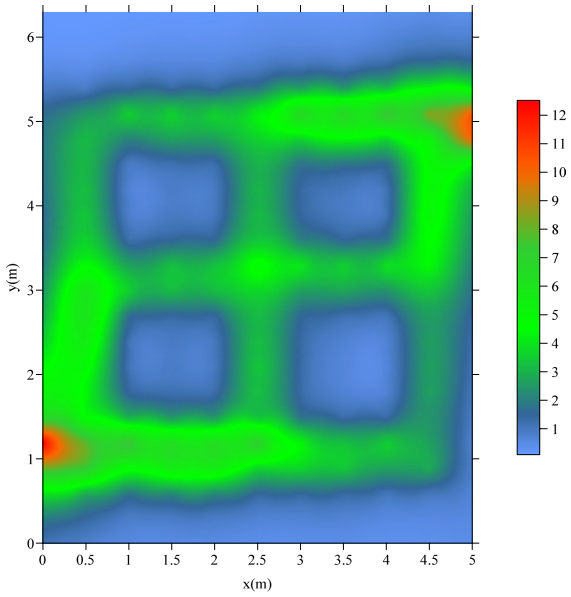

FIGURE 15. Test result on the physical model of grounding grid.

FIGURE 16. 110kv Transformer substation.

of the small physical model is known. The induced signal is measured directly alone the direction of the branch to verify feasibility. The NDT equipment measures the magnetic field data above the conductors of the grid. After each measurement, move the trolley forward on the y directions. We performed 9 measuring lines. Each measuring line includes 11 test points. The space between the measuring lines is 0.5m. Thus, there are 9 points on x-direction and 11 points on y-direction. The measured area is 4.5m×5.5m.

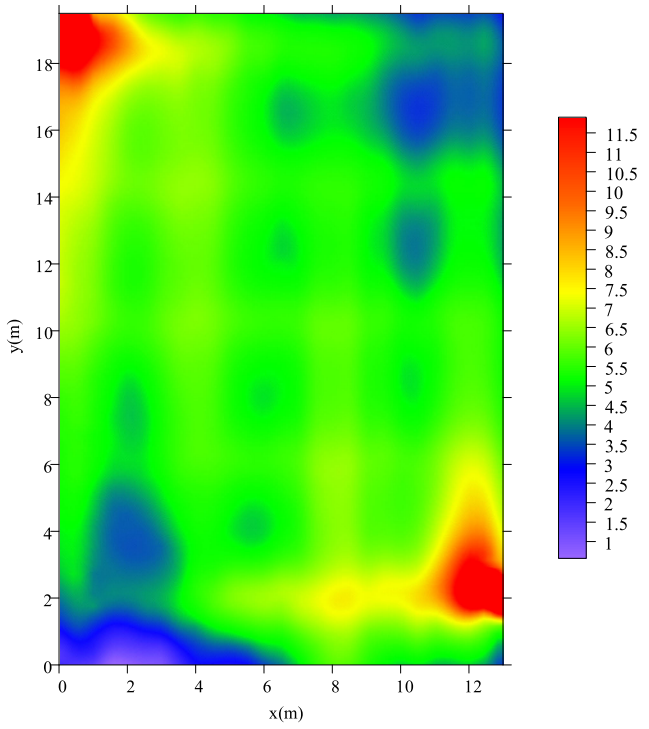

FIGURE 17. Magnetic field distribution without anti-noise process.

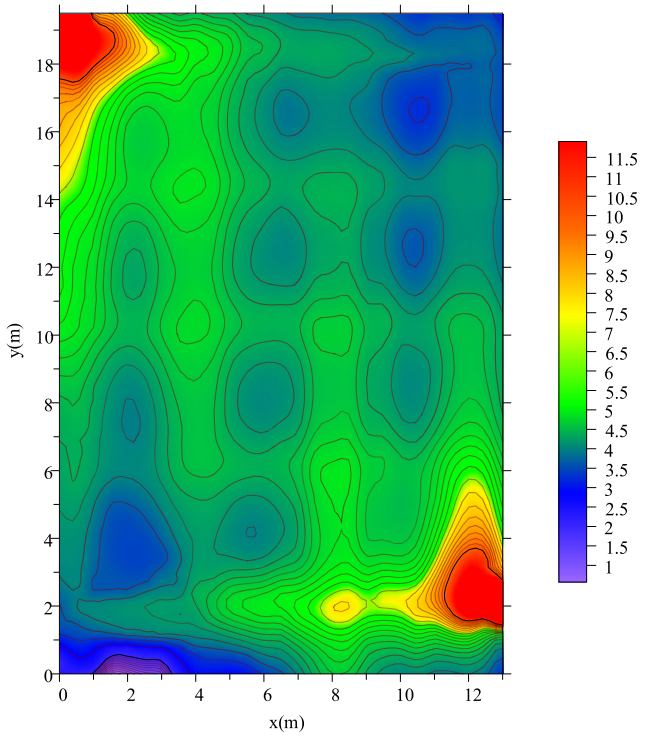

FIGURE 18. Magnetic field distribution after EEMD.

After the implementation of single-channel BSS, the induced signal was reconstructed and the magnitude of the magnetic field was calculated. The topology structure of the small physical model of the grounding grid is obtained according to the distribution of amplification and phase

FIGURE 19. Excavation to verify the correctness of result.

of the induced magnetic field at each point, as shown in Fig.15

Comparing Fig. 14 and Fig. 15, the topology structure of the distribution can be recognized clearly. The positions of the conductors are all correct.

C. EXPERIMENT IN A REAL SUBSTATION

The proposed method and the self-made equipment were further verified in a real substation shown in Fig. 16. The substation was built in the 1990s, located in the northwest of China. The grounding grid of the substation was 60mm×5mm galvanized carbon steel. The mesh was buried in soil as deep as 0.8 m. The injection electrodes were 40mm×4mm galvanized steel as designed.

We measured 13m on x-direction and 19.5m on y-direction. The measuring spacing is 0.5m on x-direction and 0.3m on y-direction. That implies 27 measuring points on x and 66 measuring points on y.

After the acquisition of the EMI signal, all the magnetic flux densities of all the 27 × 66 testing points are obtained. In order to verify the effect of the EEMD algorithm, we drew two pseudo color maps of the magnetic field distribution.

Fig.17 illustrates the magnetic field distribution drawn according to sampled data without any anti-noise process. The position and the topological structure of the grounding conductors cannot be recognized due to the strong inference around the substation. The wanted signal is buried in the unknown signal of other sources.

Fig. 18 is the map drawn according to the data after EEMD. The topological structure of the grounding grids can be clearly recognized.

In order to prove the correctness of the result of the proposed method, we excavated manually by 0.8m deep according to the position of buried conductor shown on Fig. 18. The excavation verifies that the drawn structure of grounding grids matches the facts, as shown in Fig. 19. the EEMD-based method accurately extracts the induced small signal and visualizes the distribution of the electromagnetic field even though the signal is buried in the strong noises. This result shows that the proposed method is practical in EMI signal detection in the harsh electromagnetic environment. The reconstruction ability of the diagnosis system is satisfying.

VI. CONCLUSION

This paper described a single-channel BSS scheme for EMI signal extraction and validated its performance. The EEMD-EMI method is proposed to solve the anti-interference problem in the detection to grounding grids in a harsh electromagnetic environment.

From the simulation and real-life experiment results, it is clear that the EEMD-based EMI method is effective for the extraction of signals, which makes the NDT equipment for grounding grids feasible to determinate the structure of the conductor.

ACKNOWLEDGMENT

The authors are grateful to the editors and anonymous reviewers for their constructive comments to improve this paper.

REFERENCES

[1] S. Yu, G. Dong, N. Liu, X. Liu, C. Xu, Y. Ji, and H. Luan, "Diagnosis for conductor breaks of grounding grids based on the wire loop method of the transient electromagnetic method," *Math. Problems Eng.*, vol. 2019, Mar. 2019, Art. no. 1489543.

[2] F. E. Asimakopoulou, G. J. Tsekouras, I. F. Gonos, and I. A. Stathopulos, "Estimation of seasonal variation of ground resistance using artificial neural networks," *Electr. Power Syst. Res.*, vol. 94, pp. 113–121, Jan. 2013.

[3] C. Li, W. He, D. Yao, F. Yang, X. Kou, and X. Wang, "Topological measurement and characterization of substation grounding grids based on derivative method," *Int. J. Elect. Power Energy Syst.*, vol. 63, pp. 158–164, Dec. 2014.

[4] S. Wang, J. Liu, S. Wang, and Z. Li, "Grounding grid corrosion diagnosis and uncertainly analysis of branches," *J. Comput.*, vol. 5, no. 8, pp. 1289–1295, 2010.

[5] G. Liu, G. Jiang, Z. Zhang, D. Mei, and Y. Zheng, "Research on the influence of DC current overflowing on grounding electrode corrosion," in *Proc. ITOEC*, Chongqing, China, Oct. 2017, pp. 291–295.

[6] C. Yu, Z. Fu, X. Hou, H.-M. Tai, and X. Su, "Break-point diagnosis of grounding grids using transient electromagnetic apparent resistivity imaging," *IEEE Trans. Power Del.*, vol. 30, no. 6, pp. 2485–2491, Dec. 2015.

[7] Y. Liu and X. Cui, "Measurement and analysis of conduction EMI in substation and design of power filter," in *Proc. MAPE*, Hangzhou, China, Aug. 2007, pp. 1307–1310.

[8] Y. Fan, L. Kai, Z. Liwei, Z. Songyang, H. Jiayuan, W. Xiaoyu, and G. Bin, "A derivative-based method for buried depth detection of metal conductors," *IEEE Trans. Magn.*, vol. 54, no. 4, Apr. 2018, Art. no. 6200709.

[9] L. V. Gomes, E. Macedo, E. Costa, R. Freire, and M. Castro, "Failure detection in energized high voltage substation grounding grids—A case study," *Int. J. Eng. Sci. Invention*, vol. 7, no. 5, pp. 24–35, Jul. 2016.

[10] X. Kou, M. Dong, F. Yang, S. Han, K. Zhang, L. Guo, and G. Ding, "Design of grounding grid conductor positioning device on the magnetic field method," *Prog. Electromagn. Res. M*, vol. 67, pp. 105–117, 2018.

[11] H. Liu, Z. Liu, H. Dong, J. Ge, Z. Yuan, J. Zhu, H. Zhang, and X. Zeng, "Recurrent neural network-based approach for sparse geomagnetic data interpolation and reconstruction," *IEEE Access*, vol. 7, pp. 33173–33179, 2019.

[12] X. Long, M. Dong, W. Xu, and Y. W. Li, "Online monitoring of substation grounding grid conditions using touch and step voltage sensors," *IEEE Trans. Smart Grid*, vol. 3, no. 2, pp. 761–769, Jun. 2012.

[13] A. Qamar, F. Yang, W. He, A. Jadoon, M. Z. Khan, and N. Xu, "Topology measurement of substation's grounding grid by using electromagnetic and derivative method," *Prog. Electromagn. Res. B*, vol. 67, pp. 71–90, 2016.
[14] A. Qamar, N. Shah, Z. Kaleem, Z. Uddin, and F. A. Orakzai, "Breakpoint diagnosis of substation grounding grid using derivative method," *Progr. Electromagn. Res. M*, vol. 57, pp. 73–80, 2017.
[15] A. Qamar, F. Yang, N. Xu, and S. A. Shah, "Solution to the inverse problem regarding the location of substation's grounding grid by using the derivative method," *Int. J. Appl. Electromagn. Mech.*, vol. 56, no. 4, pp. 549–558, 2018.
[16] A. Brahmi, H. Ghennioui, C. Corbier, F. Guillet, and M. Lahbabi, "Blind separation of cyclostationary sources sharing common cyclic frequencies using joint diagonalization algorithm," *Math. Problems Eng.*, vol. 2017, Feb. 2017, Art. no. 2546838.
[17] B. Gao, L. Bai, W. L. Woo, G. Y. Tian, and Y. Cheng, "Automatic defect identification of eddy current pulsed thermography using single channel blind source separation," *IEEE Trans. Instrum. Meas.*, vol. 63, no. 4, pp. 913–922, Apr. 2014.
[18] Z. Uddin, A. Ahmad, M. Iqbal, and M. Naeem, "Applications of independent component analysis in wireless communication systems," *Wireless Pers. Commun.*, vol. 83, no. 4, pp. 2711–2737, 2015.
[19] Z. Uddin, A. Ahmad, M. Iqbal, and Z. Kaleem, "Adaptive step size gradient ascent ICA algorithm for wireless MIMO systems," *Mobile Inf. Syst.*, vol. 2018, May 2018, Art. no. 7038531.
[20] G. Yang, Y. Liu, Y. Wang, and Z. Zhu, "EMD interval thresholding denoising based on similarity measure to select relevant modes," *Signal Process.*, vol. 109, pp. 95–109, Apr. 2015.
[21] Y. Lei, Z. He, and Y. Zi, "Application of the EEMD method to rotor fault diagnosis of rotating machinery," *Mech. Syst. Signal Process.*, vol. 23, no. 4, pp. 1327–1338, 2009.
[22] P. Tian, X. Cao, J. Liang, L. Zhang, N. Yi, L. Wang, and X. Cheng, "Improved empirical mode decomposition based denoising method for lidar signals," *Opt. Commun.*, vol. 325, pp. 54–59, Aug. 2014.
[23] H. Li, Y. Chen, G. Zhang, J. Li, N. Zhang, B. Du, H. Liu, and N. Xiong, "Transmission line ice coating prediction model based on EEMD feature extraction," *IEEE Access*, vol. 7, pp. 40695–40706, 2019.
[24] L. Mengting, H. Darong, Z. Ling, C. Ruyi, F. Kuang, and J. Yu, "An improved fault diagnosis method based on a genetic algorithm by selecting appropriate IMFs," *IEEE Access*, vol. 7, pp. 60310–60321, May 2019.
[25] B. Li, P. L. Zhang, Z. J. Wang, S. S. Mi, and D. S. Liu, "A weighted multi-scale morphological gradient filter for rolling element bearing fault detection," *ISA Trans.*, vol. 50, no. 4, pp. 599–608, Oct. 2011.
[26] H. Sun, H. Wang, and J. Guo, "A single-channel blind source separation technique based on AMGMF and AFEEMD for the rotor system," *IEEE Access*, vol. 6, pp. 50882–50890, 2018.
[27] Z. Wu and N. E. Huang, "Ensemble empirical mode decomposition: A noise-assisted data analysis method," *Adv. Adapt. Data Anal.*, vol. 1, no. 1, pp. 1–41, 2008.
[28] L. Pan, K. Liu, J. Jiang, C. Ma, M. Tian, and T. Liu, "A de-noising algorithm based on EEMD in Raman-based distributed temperature sensor," *IEEE Sensors J.*, vol. 17, no. 1, pp. 134–138, Jan. 2017.
[29] H. Song, H. Dong, and P. Zhang, "A virtual instrument for diagnosis to substation grounding grids in harsh electromagnetic environment," in *Proc. I2MTC*, Turin, Italy, May 2017, pp. 1–6.

HENGLI SONG received the Ph.D. degree from the Huazhong University of Science and Technology, Wuhan, China, in 2013. He was a Visiting Scholar with the University of Technology Sydney, Australia, from 2016 to 2017. He is currently a Lecturer with the School of Automation, China University of Geosciences, Wuhan. His current research interests include weak signal detection, signal processing, and geophysical instrument.

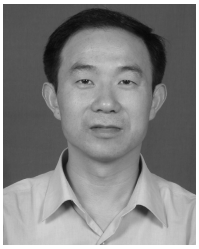

HAOBIN DONG received the Ph.D. degree from the Huazhong University of Science and Technology, Wuhan, China, in 2002. He was a Visiting Associate Professor with the Well Logging Laboratory and the Subsurface Sensing Laboratory, Department of Electrical and Computer Engineering, University of Houston, Houston, TX, USA, from 2005 to 2006. He is currently a Professor with the School of Automation, China University of Geosciences, Wuhan. His current research interests include weak signal detection and intelligent geophysical instrument.

ZHIWEN YUAN is currently a Senior Engineer with the Science and Technology on Near Surface Detection Laboratory, Wuxi, China. His current research interest includes near surface detection technology.

JUN ZHU is currently a Senior Engineer with the Science and Technology on Near Surface Detection Laboratory, Wuxi, China. His current research interest includes near surface detection technology.

HAIYANG ZHANG is currently a Senior Engineer with the Science and Technology on Near Surface Detection Laboratory, Wuxi, China. His current research interest includes near surface detection technology.

YUJIN HUANG is currently a Lecturer with the School of Automation, China University of Geosciences, Wuhan, China. His current research interest includes intelligent instrument.